

Interaction between ultrashort laser pulses and gold nanoparticles: nanoheater and nanolens effect

N. N. Nedyalkov · S. Imamova · P. A. Atanasov ·
Y. Tanaka · M. Obara

Received: 10 June 2009 / Accepted: 25 May 2010 / Published online: 18 June 2010
© Springer Science+Business Media B.V. 2010

Abstract Theoretic and experimental results on the heating process and near field localization arising when gold nanoparticles are irradiated by ultrashort laser pulses are presented. The system under consideration consists of nanoparticles with radius of 20, 40, or 100 nm in vacuum or deposited on different substrates. Substrate materials with different dielectric properties are used to sense and visualize the nanoparticle heating and near electromagnetic field distribution. The theoretic analysis is based on two-temperature heat model for estimation of the nanoparticle temperature and Finite Difference Time Domain (FDTD) method for description of the near field distribution in the vicinity of the particles. It is found that at even moderate laser fluences, particle temperature can reach a value sufficient for bubble formation in biological tissues. The analysis of the near field distribution shows that when particle is deposited on substrate surface, the dielectric properties of the substrate define the localization and enhancement of the near field intensity. The efficiency of this process determines the contribution of

particle heating or near field intensity enhancement in the surface modification process. The localization of the near field intensity in the vicinity of the contact point between the particle and substrate is proved experimentally for metal and silicon substrates, where the experimentally obtained surface modifications resemble the theoretically predicted intensity distribution.

Keywords Laser nanostructuring · Metal nanoparticles · Plasmonics · Biophotonics · Near field properties · Modeling and simulation

Introduction

Although the basic physics of the interaction between the electromagnetic field and metal particles with dimensions smaller than the incident wavelength was described already more than 100 years ago by Mie (1908, see also Kerker 1969), their unique properties have attracted significant interest recently. The development of commercial and also new reliable methods for fabrication of metal particles (Abe et al. 1998; Buscaglia et al. 2008; Chen et al. 2000; Zheng et al. 2007), and precise control of their size distribution and deposition has increased the possibility of their applications in different fields (Chu et al. 2005; Matsui 2005; Schleunitz et al. 2007). The

N. N. Nedyalkov (✉) · Y. Tanaka · M. Obara
Department of Electronics and Electrical Engineering,
Faculty of Science and Technology, Keio University,
3-14-1 Hiyoshi, Kohoku-ku, Yokohama 223-8522, Japan
e-mail: nnn_1900@yahoo.com

N. N. Nedyalkov · S. Imamova · P. A. Atanasov
Institute of Electronics, Bulgarian Academy of Sciences,
72, Tsarigradsko shose Boul., 1784 Sofia, Bulgaria

noble metal (Au, Ag) nanoparticles are especially attractive due to the possibility of efficient excitation of plasmons with the commercially available light sources in the near UV and visible regions of the spectrum (Kreibig and Vollmer 1995). The plasmon excitation in these structures is responsible for enormous enhancement of their absorption and scattering coefficients, which at resonance conditions can be increased by orders of magnitude. An important characteristic of the nanoparticles optical spectra is their dependence on the size of the particles, their shape and structure, dielectric properties of the environment, geometry of excitation, and the particles arrangement (Kelly et al. 2003; Prodan et al. 2003; Pustovalov and Babenko 2005). This gives an opportunity of tuning the resonant wavelength in a wide range that can cover the visible and even near infrared regions of the spectrum. Furthermore, gold nanoparticles express good photostability and can be easily functionalized with antibodies and proteins. These properties are the basis for their application in biophotonics where noble metal nanoparticles are used for cell processing, as cancer cell photothermal therapy (Jain et al. 2008; Lal et al. 2008; Zharov et al. 2005a, b) and cell imaging (Loo et al. 2005; Shirma et al. 2006). In the particle-mediated cell processing applications, the enhanced absorption of the particle leads to its strong heating that can result in triggering of irreversible chemical effects, or bubble formation in the material.

Besides the modification of the optical properties observed in the far field zone, the excitation of plasmons in metal nanoparticles is accompanied by the development of strong field in the near field zone (Kik et al. 2002; Plech et al. 2008). The evanescent nature of this field defines an exponential decrease of the optical intensity with the distance from the particle surface. However, when an object is placed in the near field zone of the particle, it can absorb the near field energy and can result in its modification (Huang et al. 2003; Leiderer et al. 2004; Nedyalkov et al. 2007a). Using this effect, nanosized modifications in metal, dielectric, and semiconductor materials are demonstrated (Nedyalkov et al. 2007a). The properties of the near field in the vicinity of nanoparticles are also found to depend on the particles' characteristics, environmental dielectric properties, and parameters of the incident irradiation as polarization and wavelength,

and particle arrangement (Eversole et al. 2007; Nedyalkov et al. 2006a).

Thus, the interaction of the electromagnetic field with noble nanoparticles is a complex phenomenon, and, therefore, the efficient application of its properties need a detailed investigation. This is especially valid in the field of biophotonics where the efficient and safety application need detailed knowledge of the processes involved. Up to now, the studies performed (Jain et al. 2008; Huang et al. 2003; Khlebtsov et al. 2006; Lal et al. 2008; Leiderer et al. 2004; Zharov et al. 2005a, b) have investigated the particle absorption and heating, and the near field properties separately, which have limited the overall understanding of the interaction, where generally both these effects play a role.

In this article, we present a theoretic and experimental investigation on two main effects arising when gold nanoparticles interact with electromagnetic field. The first one is energy absorption and nanoparticle heating (nanoheater effect) described by combination of optical properties calculation by Mie theory and two-temperature heat model. The second one is related to the ability of the nanoparticle to concentrate energy in its vicinity (nanolens effect), and in general the properties of the electromagnetic field in the near field zone. In such a way, we give more detailed view of the nanoparticle–laser pulse interaction. Ultrashort laser pulses at wavelength of 800 nm are used in this study. From the viewpoint of practical applications, the ultrashort irradiation offers a possibility of minimizing the heat-affected zone and can significantly contribute to a strong localization of the laser–matter interaction. When interaction of such pulses with nanoparticles is considered, the heat diffusion to the surrounding medium is negligible during the laser pulse which ensures efficient particle heating. The wavelength of the used laser irradiation falls into the transparent window of the human tissue (600–1300 nm, Vo-Dinh 2003), and the obtained results can be applied in designing technique for in vivo processing of biological objects. We show the conditions that influence the efficiency of particle heating and the role of enhanced near field. The realization of the two mechanisms is demonstrated experimentally by producing permanent modifications of different substrates. The results indicate that at certain conditions, the role of the local field enhancement in particle vicinity dominates the

substrate modification characteristics over the nanoparticle heating.

Simulation model

For reliable description of the nanoparticle heating process, optical parameters of the nanoparticle should be obtained. In this study, the absorption cross section is obtained on the basis of Mie scattering theory using the following equation:

$$C_{\text{abs}} = C_{\text{ext}} - C_{\text{sca}}, \tag{1}$$

where C_{ext} and C_{sca} are the extinction and scattering cross sections given by Papavassiliou (1979):

$$C_{\text{ext}} = \frac{4\pi R^2 \epsilon_m^{3/2}}{\lambda a^3} \sum_l (2l + 1) \text{Re}(A_l + B_l) \tag{2}$$

$$C_{\text{sca}} = \frac{4\pi R^3 \epsilon_m^{1/2}}{\lambda a^3} \sum_l (2l + 1) (|A_l|^2 + |B_l|^2) \tag{3}$$

Here, λ is the wavelength of the incident irradiation, ϵ_m is the dielectric function of the surrounding medium, $a = (2\pi R \epsilon_m^{1/2})/\lambda$, R is the particle radius, and A_l and B_l are the electric and magnetic partial oscillation coefficients. The optical parameters for gold used in the calculation are taken from Johnson and Christy (1972).

The temperature evolution of the particle during and after the interaction with the laser pulse is traced by one-dimensional two-temperature model (Pustovalov 2005):

$$C_e \frac{\partial T_e}{\partial t} = -\gamma(T_e - T_i) + S \tag{4}$$

$$C_i \frac{\partial T_i}{\partial t} = \gamma(T_e - T_i) \tag{5}$$

$$S = IC_{\text{abs}}/V_p \tag{6}$$

Here, T_e and T_i are the electron and lattice temperatures (Anisimov et al. 1974, see also for example von Allmen 1987), S and I are the laser energy source and laser intensity (time dependent), respectively; $V_p = 4/3\pi R^3$ is the particle volume; C_i , C_e , and γ are the lattice and electron system heat capacities, and electron-lattice coupling constant, respectively. In this model, the spatial distribution in the particle heating is neglected, and it is assumed to be homogeneous. In order to clarify the validity of this

assumption, 2D model is also applied for description of nanoparticle heating. In this model, the system of equations is modified as heat flux terms in the form: $-k_{e(i)}(\nabla T_{e(i)})$ for electron, and lattice systems are added in the right side of the Eqs. 4 and 5. For the source term, the relation $S = \sigma E^2(t)$ is used (Habash 2007), where σ is the gold conductivity. The electric field intensity $E^2(t)$ values are taken from the FDTD simulation which is described shortly.

Since the heat transfer between the particle and the surrounding medium has a characteristic time of few tens of picoseconds (Link and El-Sayed 1999), this process is neglected in the calculation of the particle temperature. The coupled equation Eqs. 4–6 and 2D modification are solved using a classical finite difference scheme and by taking into account the temperature dependence of the electron heat capacity according to $C_e = A_e T_e$, where $A_e = 70 \text{ J/m}^3\text{K}^2$, and the temperature dependence of C_i (Chowdhury and Numer 2003).

The electron heat conductivity of gold is assumed to be constant, as the value of $2 \times 10^3 \text{ W/mK}$ is used as average obtained from the expression $k_e = k_{e0}(T_e/T_i)$, with the electron temperature range from 300 to 9000 K, and $k_{e0} = 318 \text{ W/mK}$ (Wellershoff et al. 1999). The lattice heat conductivity of gold k_i is 318 W/mK . The value of the coupling coefficient, $\gamma = 3.10^{16} \text{ W/m}^3\text{K}$ is taken from Hodak et al. (1998).

The electric field distribution and the optical near field enhancement in the vicinity of nanoparticles are calculated by the Finite FDTD method (Taflove and Hagness 2000). This method is a numerical algorithm for solving Maxwell’s equations, and it allows a solution of electromagnetic distributions for complex geometries and inhomogeneous systems. In this model, the simulated system is divided into elementary cells, where the electric and magnetic field components are calculated at each time step. The dielectric function of the gold particles is described by Drude model as the input parameters are taken from Johnson and Christy (1972) and Vial et al. (2005). Simulations are made for the system consisting of gold nanoparticle in vacuum or placed on the dielectric substrate with refractive index of 1.488 corresponding to polymethyl methacrylate (PMMA) (Baker and Dyer 1993), and silicon and platinum (Pt) film. The dielectric functions of silicon and platinum are taken from Palik (1998). These materials are chosen due to their different dielectric properties

which play a crucial role for the characteristics of the near field intensity distribution as it will be shown shortly. The electric field intensity which is an input parameter for FDTD simulation is assumed to be 1 (V/m)^2 in all simulations.

In this study, results for gold nanoparticle with radius of 20, 40, and 100 nm are shown. According to the calculations for the near field scattering efficiency (Messinger et al. 1981), particles in this size range show strong enhancement of the near field intensity. Furthermore, particles with dimensions in this range are usually objects of investigation in the area of nanoparticle-assisted photothermal therapy (Khlebtsov et al. 2006).

Experimental details

Gold spherical particles with radius of 100 nm dispersed in water (BBInternational Corp.) are used in the experiments. The particles are deposited on different substrates by spin-coating method. After deposition, the particles are randomly distributed on the substrate surface. The experiments are performed with a Ti:sapphire chirped pulse amplification system (Thales laser) that produces 1 mJ pulses at a repetition rate of 1 kHz and center wavelength of 800 nm. The laser pulse duration is 100 fs (full width at half maximum). The laser radiation is directed normally to the surface and is focused by a lens with focal length of 250 mm. The spot size on the substrate surface is estimated to be about 100 μm . The pulse energy is adjusted by a variable attenuator. The experiment is done on a single shot basis, as the shot number is controlled by a high-speed mechanical shutter. For the experiments with circular polarization, a quarter-wave plate is used for transformation.

For sensing the particle heating and the near field properties in their vicinity, PMMA, thin Pt film, and silicon are used as substrates in the experiments. The substrate materials are chosen to have different dielectric properties to estimate its role on the investigated effects. The refractive index of PMMA substrate is close to the typical for bio-tissue, and the results can be used in biophotonics. In addition, the modification technique shown here can be used in a lithography technology efficiently for materials having a variety of applications such as metal films and silicon. The Pt thin film with thickness of 20 nm, deposited by ion sputtering is used. The roughness of

the substrates is estimated as 4 nm (RMS) for PMMA and metal film, and 1 nm for Si. After laser irradiation, the samples are not treated to remove gold particles.

The irradiated samples are analyzed by AFM (SPA300/SPI3800, Seiko Instruments Inc.) and SEM (Sirion 400, FEI Company).

Results and discussion

Gold nanoparticles as nanoheater

Figure 1 represents the absorption cross-sectional spectra of single gold nanoparticles with radius of 20, 40, and 100 nm calculated by Eqs. 1–3. The clearly expressed peaks in the absorption cross sections are related to plasmon excitation in the nanoparticles. The maximal values are observed in the range of about 525–550 nm for particles with radius $R = 20$ and 100 nm. The values of the absorption cross sections at wavelength of 800 nm are about two orders of magnitude lower than the optimal ones for particles with $R = 20$ and 40 nm. Although, the increase of the particle dimensions results in the broadening of the plasmon absorption band and a shift of the maxima to the longer wavelengths, the value of the cross section for particle with radius 100 nm is about 20 times lower than the peak value. Using the calculated absorption cross sections, the temperature

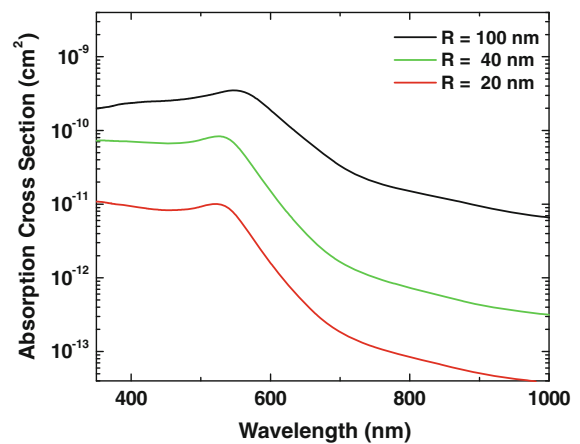


Fig. 1 Absorption cross-sectional spectra of single gold nanoparticles in vacuum with radius of 20, 40, and 100 nm calculated by Eqs. 1–3

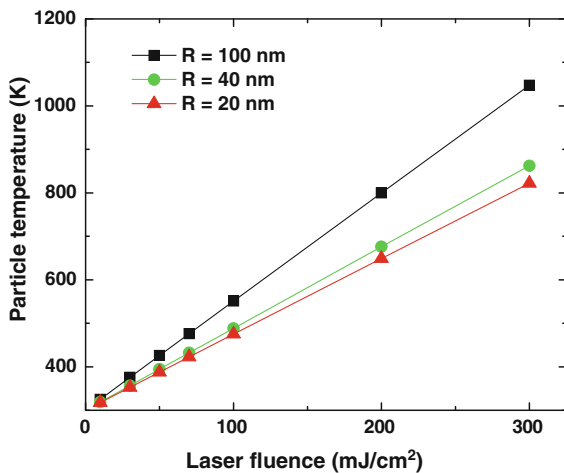


Fig. 2 Calculated dependence of the maximal temperature reached in the nanoparticles with different diameters as a function of the applied laser fluence. The incident irradiation is a single laser pulse with duration of 100 fs at wavelength of 800 nm. The data are obtained from Eqs. 4–6 using results shown in Fig. 1

of the particles is obtained using the two-temperature diffusion model. The values of the maximal temperature reached in the nanoparticles when they are irradiated by a single 100 fs laser pulse as a function of the incident laser fluence are shown in Fig. 2. For comparison, the value of the maximal temperature obtained at the highest absorption (at $\lambda = 550$ nm) for $R = 100$ nm particle exceeds 5×10^3 K at fluence of 100 mJ/cm^2 . It should be noted that for biophotonic applications, such as cell membrane modification, the necessary increase of the temperature should be up to about 315 K (42 °C) (Liu et al. 2008) and kept for a certain period of time, especially when CW or high repetition rate (tens of MHz) laser systems are used. For more strong interaction, when irreversible cell modification is based on bubble formation (as in tumor cell killing), the necessary temperature should be at least 470 K (Volkov et al. 2007; Zharov et al. 2005a, b). When ultrashort laser pulses are used, such heating is realized in nearly isochoric conditions which will result in the development of significant tensile stress (Vogel et al. 2007) in the vicinity of the heating point. This will lead to the formation of a cavitation bubble without the need of heat accumulation, i.e., after single pulse. From Fig. 2, it is seen that a temperature of 470 K can be achieved by the gold nanoparticles with the sizes assumed in this study after single laser pulse, at fluences of about 70 mJ/cm^2

for $R = 100$ nm and at 100 mJ/cm^2 for particles with $R = 20$ and 40 nm. It should also be mentioned that experimentally obtained threshold for biological cell modification (the example is for human breast MDA–MB cell, Cho et al. 2008) using direct femto-second laser pulse irradiation (without nanoparticle mediation) is estimated to be about 500 mJ/cm^2 .

The investigation on the light scattering by gold nanoparticles shows that the near field spatial distribution in the vicinity of the particle is complex and consists of radial component of the electric field (Messinger et al. 1981; Quinten 1995). Complex spatial distribution is also observed for the energy flow toward, and out of, the particle (Bashevoy et al. 2005; Wang et al. 2004). It can be expected that the inhomogeneous energy deposition into the particle will result in its inhomogeneous heating. In order to clarify this, 2D two-temperature heat diffusion model is applied to describe the particle heating process. Figure 3 represents the temporal evolution of the electron temperature at two points in the particle with $R = 100$ nm at considered incident laser fluence of 100 mJ/cm^2 . The electric field intensity corresponding to this fluence is used as incident for FDTD simulation. The predicted values from this simulation are then used in the source term, S , in the heat equations. The FDTD simulation predicts a complex spatial distribution of the energy deposited into the particle. This results in a spatial nonhomogeneity of the initial temperature distribution. The points P1 and P2, in which temperature evolution is traced, are located at the points of the maximal and minimal temperature, respectively, achieved at the end of the laser pulse, respectively. The inset in Fig. 3 shows a color map of the electron temperature of the particle taken at 0.4 ps after the laser pulse onset. At this moment, where the laser pulse action accomplishes, the temperature at the particle surface and at the particle center differs by a factor of 2. Owing to the electron heat diffusion, however, the electron temperature equilibrates within the particle in the frame of about 0.5 ps after the laser pulse onset at the selected conditions. Since the electron–lattice thermal equilibrium is observed at about 10 ps after the laser pulse onset at the selected conditions, the heating of the particle can be assumed as *homogeneous*. Although, the model predicts fluence dependence of the electron–lattice equilibration times, in all simulations with fluences

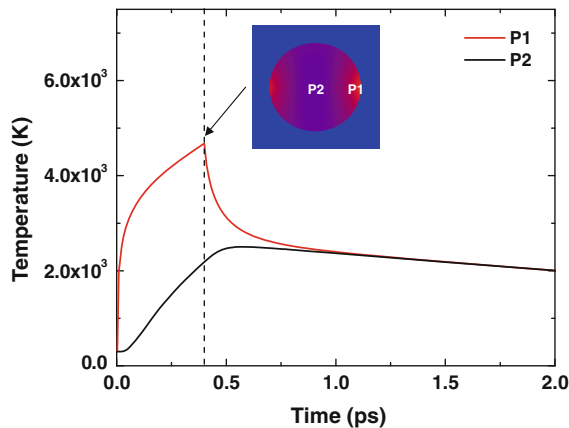


Fig. 3 Time evolution of the electron temperature at two points (P1 and P2) in the particle at considered incident laser fluence of 100 mJ/cm^2 . The spatial distribution of the absorbed energy is taken from FDTD simulation. The polarization of the incident irradiation is circular. P1 and P2 are located at the points of maximal and minimal temperature, respectively, achieved at the end of the laser pulse. The inset in the figure shows a color map of the electron temperature taken at 0.4 ps after the laser pulse onset

in the range of $10\text{--}500 \text{ mJ/cm}^2$, the electron equilibration is at least one order of magnitude faster than the electron–lattice one, i.e., particle heating can be assumed as homogeneous.

Gold nanoparticles as nanolens

The excitation of plasmons in gold nanoparticles is associated with the development of enhanced near field in their vicinity. Thus, in addition to the particle heating, the field localization in its vicinity can also contribute to the surrounding material processing. The spectrum of near field scattering efficiency (which is proportional to the power scattered in the near field zone) for gold nanoparticles shows (Messinger et al. 1981) that dipole peak shifts from visible to IR spectral range with the increase of the particle radius. Thus, at the wavelength used in this study, the near field characteristics could play an effective role for modification of a material placed in the close vicinity of the particle. Figure 4 shows the electric field intensity distribution in the vicinity of nanoparticles with radius of 20, 40, and 100 nm in vacuum calculated by FDTD simulation at incident wavelength of 800 nm. The incident irradiation has circular polarization. As can be

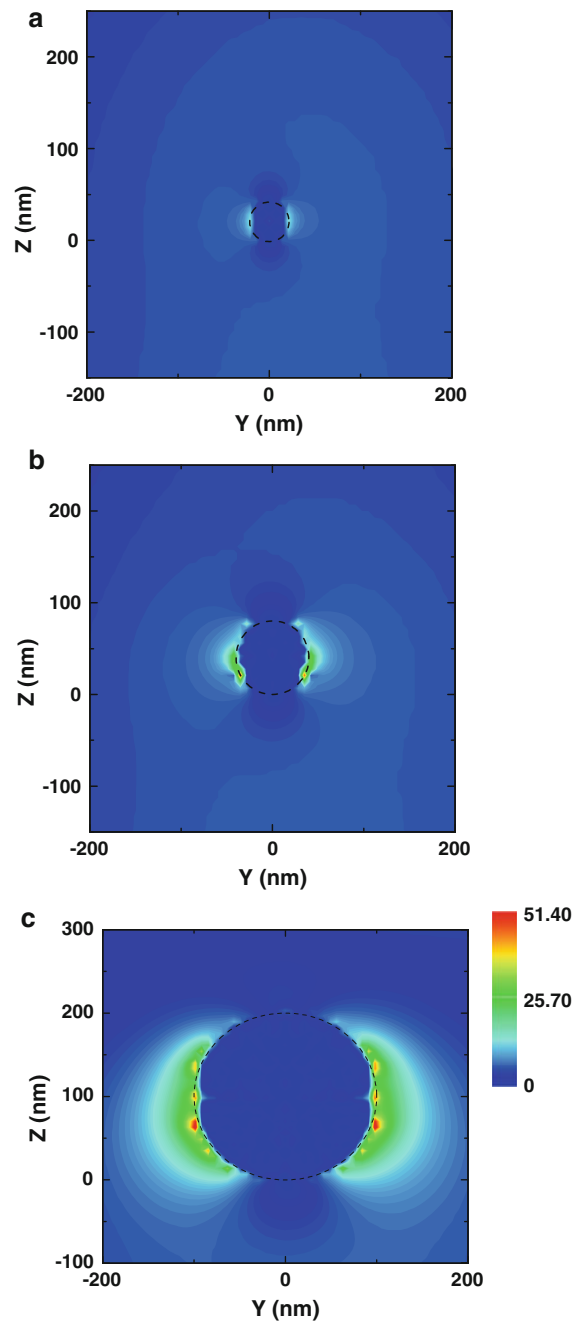


Fig. 4 Electric field intensity distribution in the vicinity of nanoparticles with radius of **a** 20 nm, **b** 40 nm, and **c** 100 nm in vacuum calculated by FDTD simulation at incident wavelength of 800 nm. The incident irradiation is considered circularly polarized plane wave with wave vector directed to Z. The electric field intensity is normalized to the incident one. *Black dashed line circles* represent particle delineation

seen from the figure, the field intensity is enhanced, and at the present configuration, the maximal value is localized in the vicinity of the equatorial plane of the particle while it is equal to the incident one at the poles of the sphere. The field distributions for particle with $R = 40$ and 100 nm show contribution of excitation of higher modes than those for the dipole one can do. The results indicate that the intensity field enhancement at the wavelength considered is maximal (about 50 times with respect to the incident one) for the biggest particle used in this study, i.e., for $R = 100$ nm, where the plasmon excitation is efficiently red shifted. Figure 5 represents the case where the particle with radius of 100 nm is placed on the dielectric substrate with refractive index of 1.488 , silicon substrate, and on platinum substrate. The presence of the substrate changes the near field spatial distribution in the particle vicinity, and the zone with the maximal intensity is shifted in direction to the substrate compared to the case of homogeneous vacuum environment (nanolens effect). While this effect is not clearly expressed in the case of the dielectric substrate where the maximal value is still not localized on the substrate surface, in the case of silicon and metal substrates, the maximal field intensity is localized in the vicinity of the contact point between particle and the substrate. This effect is related to the change of the near field scattering pattern which the substrate induces through contribution of excitation of higher plasmon modes (quadrupole mode excitation in the case of Si substrate is evident) and interaction between charges on the particle and image ones induced in the substrate (Nedyalkov 2006b).

Thus, the localization and enhancement of the field in the vicinity of the nanoparticles express a wide range of properties that can be used in modification of materials located in the particle near field zone. As it is shown, when nanoparticle is deposited on a substrate and the incident irradiation is incoming normally to the substrate surface, the efficient field localization and intensity enhancement on the substrate surface strongly depend on the dielectric properties of the substrate material. The simulations made for dielectric substrates with different refractive indices show that the effect of near field localization in the vicinity of the contact point between the particle and the substrate becomes more pronounced (and therefore the value of the field intensity on the substrate surface increases) with the increase of the

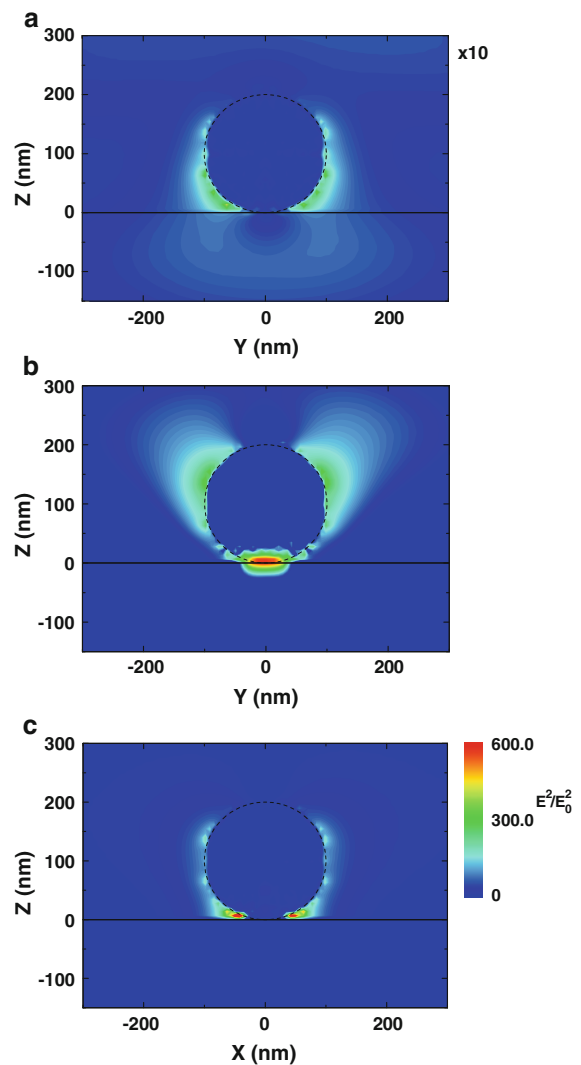


Fig. 5 Electric field intensity distribution in the vicinity of nanoparticle with radius of 100 nm placed on **a** dielectric substrate with refractive index of 1.488 , **b** silicon substrate, and **c** on platinum substrate. The intensities are scaled with respect to the case of platinum substrate, whereas for the case of dielectric substrate, it is multiplied by a factor of 10 . *Black dashed line circles* represent particle delineation, and *black line* shows the position of the substrate

refractive index of the substrate. Clear localization of the zone with the maximal field intensity on the substrate surface is observed for material with refractive index higher than 1.7 . The tendency for field localization and intensity increase with the increase of the substrate's refractive index is confirmed for the case of Si substrate where the real part of the refractive index is as high as 3.688 and the

imaginary one is 6×10^{-3} at 800 nm (Palik 1998). This validates the idea that field localization is related to the electric coupling between the particle's charge and its image charge induced in the substrate. The value of the image charge is proportional to the refractive index of the substrate material. In the field of biophotonics application, one should keep in mind that refractive indices of most soft tissues are in the range of 1.35–1.6 (for example for cell membrane is 1.46) (Vo-Dinh 2003). In addition, if the nanoparticle–substrate system is immersed in medium, the field localization and intensity enhancement on the substrate decreases with the increase of the refractive index of the surrounding medium. In such a case of low coupling with the substrate, the effect of the illumination conditions on the near field properties should be used to enhance the efficiency of nanoparticle application. For example, the change of the angle of the incident irradiation can change the magnitude of the field intensity on the substrate surface (Miyanishi et al. 2009).

The separation of the two mechanisms of nanoparticle-assisted surface modification is important due to the fact that for nanoparticles the maximum in the absorption spectra, which is related to the efficient heating of the particle, is not necessary to coincide with the maximum of the near field scattering efficiency. In the case of gold, the contribution of *d* and *sp* band electronic transitions defines high absorption at wavelengths lower than about 530 nm, and the absorption maximal position exhibits a weak dependence on the particle sizes (Messinger et al. 1981). In the wavelength range from 520 to 900 nm, the imaginary part of the complex refractive index of gold is the lowest (Kreibig and Vollmer 1995), contributing to the possibility of efficient excitation of the plasmon mode in this spectral range and efficient near field scattering. Thus, the change of the particle size results in the efficient shift of the plasmon resonance even in the IR region of the spectrum which can result in the existence of enhanced field intensity in the particle vicinity. In Fig. 6, the near field distributions in the vicinity of the gold nanoparticle with $R = 100$ nm irradiated at wavelengths of 900 and 1000 nm are shown. As it can be seen, the enhancement of the intensity is similar to that at 800 nm, i.e., the effect is noticeable at IR region where the tissue transparency window is present.

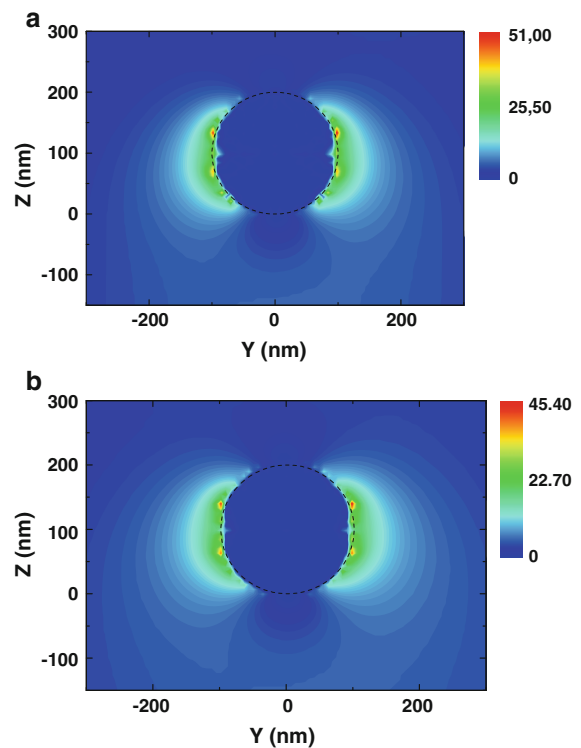


Fig. 6 Electric field intensity distribution in the vicinity of nanoparticle with radius of 100 nm in vacuum calculated by FDTD simulation at incident wavelength of **a** 900 nm, and **b** 1000 nm. *Black dashed line circles* represent particle delineation. The polarization of the incident irradiation is circular

In order to validate the theoretic results, experiments on modification of substrates with assistance of nanoparticles are performed. The theoretic results indicate that for dielectric substrate with refractive index of 1.488, the near field intensity is not localized in the vicinity of the contact point between the substrate (Fig. 5a) and the particle, and its possible modification could be related to particle heating at normal incidence. Recent results (Nedyalkov et al. 2006a, b) show that the shape of the nanoholes formed under gold nanoparticles deposited on Si (strong coupling with the substrate) follows the shape of the near field intensity distribution on the substrate surface as predicted by FDTD simulation. The latter is defined by the polarization of the incident irradiation. As a result, when circular polarization of the incident irradiation is used, the hole shape has high radial symmetry, while the application of linearly polarized irradiation results in formation of holes

with shape elongated along the polarization direction. Figure 7 shows the deposited gold nanoparticles with $R = 100$ nm on PMMA substrate before the irradiation. Figure 8 shows a modification of PMMA substrate when gold nanoparticles with $R = 100$ nm are deposited on it and the system is irradiated by a single ultrashort laser pulse with fluence of 60 mJ/cm^2 . The incident irradiation has linear polarization. According to the numerical model, the maximal temperature achieved with this fluence is

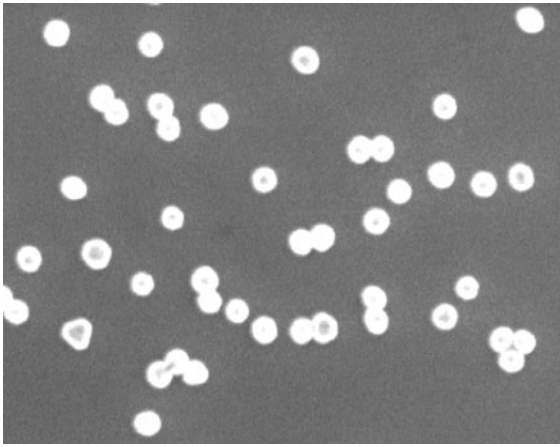


Fig. 7 SEM image of PMMA substrate when gold nanoparticles with radius of 100 nm are deposited on it. The image is taken before laser irradiation

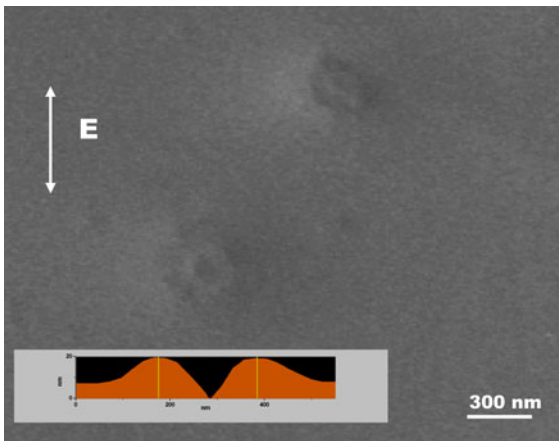


Fig. 8 SEM image of PMMA substrate when gold nanoparticles with radius of 100 nm are deposited on it, and the system is irradiated by a single ultrashort laser pulse with fluence of 60 mJ/cm^2 . The polarization of the incident irradiation is linear, and the polarization direction is shown by the arrow. The inset shows the modification area profile obtained by AFM analysis

about the melting temperature of the PMMA substrate (440 K). The observed modification has high radial symmetry, and the rest of the substrate remains unchanged which confirms the idea of local interaction only under the particle. The formation of hole at this fluence and ejection of the nanoparticle, however, suggest for more intensive interaction that leads to the substrate ablation. Such interaction can be related to the fact that the presence of substrate modifies the absorption cross section of the particle resulting in its higher temperature. Since the Mie theory cannot be applied for the system of particle–substrate and the absorption cross section cannot be obtained directly, a calculation is performed in which particle is assumed to be in homogeneous environment with an effective dielectric function. According to Kreibig and Vollmer (1995), it can be given as $\epsilon_m = 1/2(\epsilon + \epsilon_{\text{sub}})$, where ϵ_{sub} is the dielectric function of the substrate, and vacuum ($\epsilon = 1$) is assumed to surround the sphere–substrate system. For the substrate with refractive index of 1.488, the model predicts a larger temperature increase of about 100 K than that of vacuum environment.

In the case of PMMA substrate, clear dependence of the nanohole shape on the polarization of the incident irradiation is not observed in the fluence range up to the modification threshold of the native substrate. This is an evidence for the fact that the heating has the main contribution to the substrate modification. Owing to the low localization of the near field in the contact point (Fig. 5a), the nanolens effect here is negligible. The effect of near field contribution, however, is clearly seen in the case of Pt and silicon substrates. Figure 9a shows an SEM image of the modified surface of Pt film when the applied laser fluence is 20 mJ/cm^2 and the polarization of the incident irradiation is linear (the polarization direction of the incident irradiation is shown by an arrow). The electric field intensity distribution on the substrate surface is also shown in the inset (the initial distribution of the nanoparticles on the substrate surface is similar to that shown in Fig. 7). In the case under study, the shape of the modified area corresponds to the field intensity distribution, and the film is perforated at positions corresponding to the hot spots predicted from FDTD simulation. The correspondence of the near field intensity spatial distribution with film modification pattern shows that at the conditions of this study, the enhancement of the

near field under the gold particle is the governing mechanism for surface modification rather than particle heating. When circular polarization of the incident irradiation is used, the hole shape formed shows good radial symmetry, which is also in a good agreement with the simulation results (Fig. 9b). Similar results are obtained when silicon substrate is used (Nedyalkov et al. 2006b, 2007b). Although the modification mechanism for metal substrate at the conditions of this study cannot be defined precisely, one may assume that the strong electric field enhancement in the vicinity of the particle–substrate contact point may lead to the realization of a non-thermal mechanism such as electric field evaporation (Jerisch and Dickmann 1996; Park et al. 2006), or that it is responsible for the formation of initial

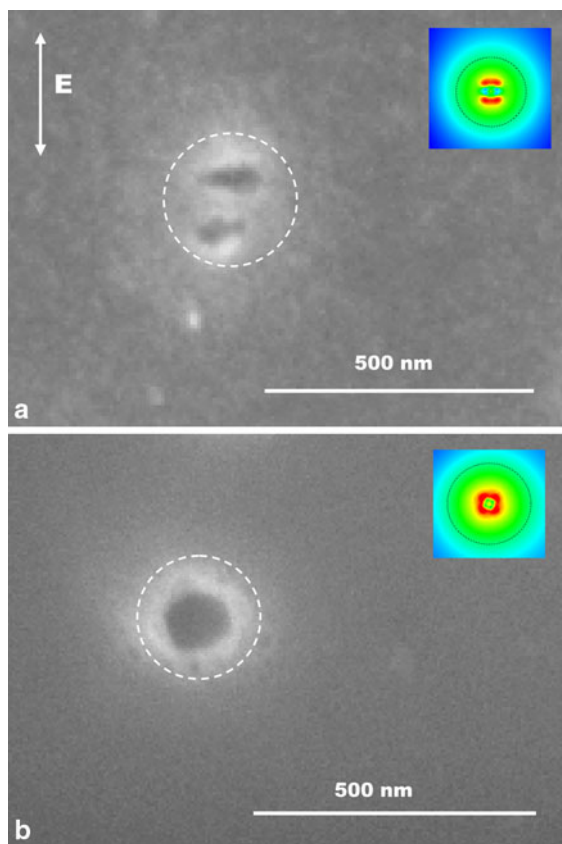


Fig. 9 SEM image of the modified surface of Pt film when applied laser fluence is 20 mJ/cm^2 , and the polarization of the incident irradiation is **a** linear (the polarization direction of the incident irradiation is shown by the *arrow*), and **b** circular. The nanoparticles used are of radius 100 nm . The calculated electric field intensity distribution on the substrate surface is also shown in the *inset*

defects in the surface. Owing to the high electron thermal conductivity of the metal, spatial distribution of the initial energy at pure thermal process will be lost within a time interval of picoseconds, and structure that is observed in Fig. 9a) is unlikely to be obtained.

If no specific treatment of the gold colloid is taken, particle tends to coalesce, leading to the formation of nanoparticle clusters. Although the description of the optical properties of nanoparticle array needs a different treatment than that for the isolated particle, we briefly mention some specific properties that are related to this study. When nanoparticles are closely spaced or they form clusters, plasmon coupling takes place. This results in the significant broadening of the absorption band and red-shifting of the absorption maxima. This effect is considered to enhance the efficiency of the application of nanoparticles in photothermal applications in the optically transparent window of human tissue (Khlebtsov et al. 2006).

The plasmon coupling realization will also influence the near field distribution in a nanoparticle array. Figure 10a shows the calculated intensity distribution on platinum substrate under nanoparticle array consisting of 64 particles. Figure 10b represents a cross-sectional view of the near field intensity distribution in the vicinity of a particle chain from the array. White circles show the particle delineations. The circular zones in Fig. 10a represent the areas with higher field intensity under the gold nanoparticles. The maximal enhancement here is about 50. From Fig. 10b, however, it is seen that the zone with the maximal field intensity is localized *between* particles, where some “hot spots” are formed. The intensity value here is higher by more than an order of magnitude than that under the particles, i.e., on the substrate surface. This phenomenon is also expressed for different substrate materials, from dielectrics to metals (Nedyalkov et al. 2007a). A comparison with the case of single, isolated particle deposited on Pt substrate (Fig. 5c) shows that the field intensity in the vicinity of the contact point between particle and the substrate is about an order of magnitude lower for array structure. This can explain the observed selective ablation of single nanoparticles and nanohole formation observed experimentally. Figure 11a shows an SEM image of Pt substrate with deposited gold nanoparticles with $R = 100 \text{ nm}$ and irradiated by a single laser pulse with fluence of 20 mJ/cm^2 .

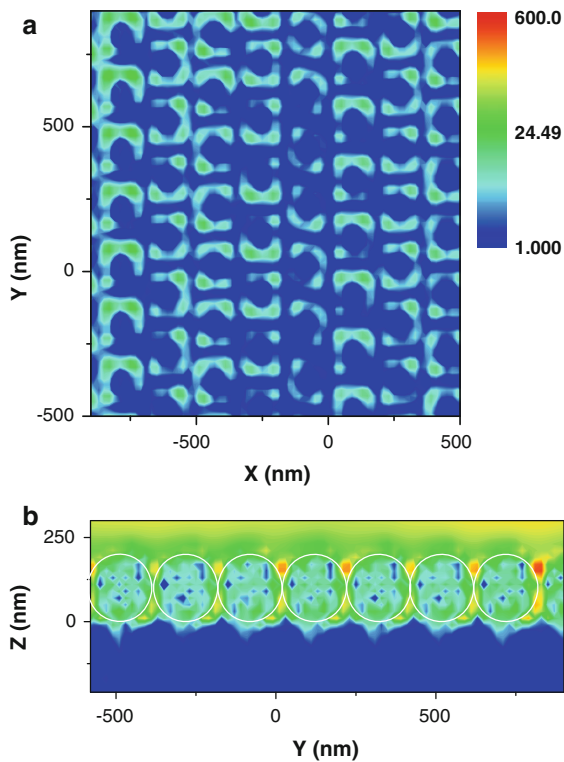


Fig. 10 Electric field intensity distribution in the vicinity of closely packed nanoparticle array consisting of 64 particles with radius of 100 nm placed on platinum substrate. **a** Shows the intensity distribution on the substrate surface. **b** Represents the intensity distribution in a cross section through a particle chain within the array. The polarization of the incident irradiation is circular

It is seen that the nanoparticle cluster formed in the deposition process remain on the substrate after the laser irradiation, while single nanoparticles are ejected and nanoholes are formed. The increase of the laser fluence results in cluster ejection and traces of substrate melting are observed (Fig. 11b). Thus, for surface modification applications, the near field localization and intensity enhancement for array structure will have a weak contribution. Instead, cluster heating will be a dominant mechanism.

Conclusions

The mechanisms of interaction of electromagnetic wave with gold nanoparticles are investigated on the basis of theoretic modeling and experiments. In relation to practical applications, the incident source

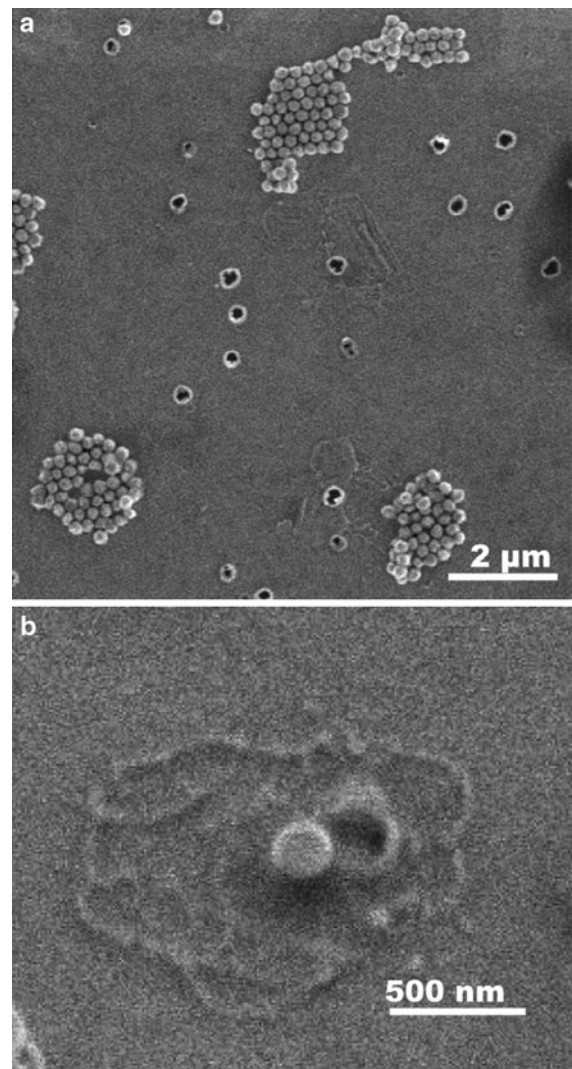


Fig. 11 **a** SEM image of Pt substrate with deposited gold nanoparticles with radius of 100 nm and irradiated by a single laser pulse with fluence of 20 mJ/cm². **b** Laser fluence is 40 mJ/cm²

is assumed to be ultrashort laser pulse at wavelength of 800 nm. The heating of nanoparticles is described by 1D two-temperature diffusion model and a model combining 2D heat diffusion model with FDTD model, which predicts the electromagnetic field distribution in the particle. The most efficient heating is obtained for the biggest particle used in this study having $R = 100$ nm. It is found that at even moderate laser fluences, its temperature can reach a value which is assumed to lead to bubble formation in biological tissues. The two-temperature model shows

that due to the electron heat diffusion, the particle is heated homogeneously; even the initially absorbed energy shows inhomogeneous distribution. The particle electron temperature equilibration time is found to be less than 1 ps, which is at least one order of magnitude lower than electron–lattice equilibration time.

The study of the near field properties in the particle vicinity shows efficient localization and intensity enhancement in the near field zone. When particle is deposited on the substrate surface, the substrate dielectric properties define the spatial distribution and enhancement of the near field intensity. For dielectric substrate with refractive index of 1.488, the zone with the maximal value of the field intensity is not localized in the vicinity of the contact point between the particle and substrate at normal incidence, and one should expect that particle heating can be a dominant mechanism for substrate modification. With the increase of the substrate refractive index, the field localization on the substrate surface is more pronounced. When silicon and platinum substrates are assumed, the intensity distribution shows strong localization of the zone with the maximal enhancement in the vicinity of the contact point between the particle and substrate.

Using the dependence of the near field properties on the characteristics of the incident irradiation, the theoretic results obtained are confirmed experimentally.

We believe that the results obtained will contribute to improving further on the recent efforts of obtaining detailed description of the properties of nanoparticles and their application in the field of biophotonics and near field optics.

Acknowledgments The authors would like to acknowledge the financial support received from Grant-in-Aid for the Global COE for High-Level Global Cooperation for Leading-Edge Platform on Access Spaces from MEXT in Japan, and Bulgarian Science Fund, under the contract D0 02-293.

References

- Abe K, Hanada T, Yoshida Y, Tanigaki N, Takiguchi H, Nakamoto M, Yamaguchi T, Yasea K (1998) Two-dimensional array of silver nanoparticles. *Thin Solid Films* 327–329:524–527
- Anisimov SI, Kapeliovich BL, Perel'man TL (1974) Electron emission from metal surfaces exposed to ultrashort laser pulses. *Eksp Teor Fiz* 66:776–781 (in Russian)
- Baker AK, Dyer PE (1993) Refractive-index modification of polymethylmethacrylate (PMMA) thin films by KrF-laser irradiation. *Appl Phys A* 57:543–544
- Bashevoy MV, Fedotov VA, Zheludev NI (2005) Optical whirlpool on an absorbing metallic nanoparticle. *Opt Express* 1:8372–8379
- Buscaglia MT, Buscaglia V, Viviani M, Dondero G, Röhrig S, Rüdiger A, Nanni P (2008) Ferroelectric hollow particles obtained by solid-state reaction. *Nanotechnology* 19: 225602
- Chen XY, Li JR, Jiang L (2000) Two-dimensional arrangement of octadecylamine-functionalized gold nanoparticles using the LB technique. *Nanotechnology* 11:108–111
- Cho S, Chang W, Kim J, Whang K, Choi K, Sohn S (2008) In situ observation of photo-bleaching in human single living cell excited by a NIR femtosecond laser. *Appl Surf Sci* 254:3370–3375
- Chowdhury IH, Numer X (2003) Heat transfer in femtosecond laser processing of metal. *Heat Transf A* 44:219–232
- Chu T, Liu W-C, Tsai D (2005) Enhanced resolution induced by random silver nanoparticles in near-field optical disks. *Opt Commun* 246:561–567
- Eversole D, Luk'yanchuk B, Ben-yakar A (2007) Plasmonic laser nanoablation of silicon by the scattering of femtosecond pulses near gold nanospheres. *Appl Phys A* 89: 283–291
- Habash RWY (2007) Bioeffects and therapeutic applications of electromagnetic energy. CRC Press, New York
- Hodak JH, Martini I, Hartland GV (1998) Spectroscopy and dynamics of nanometer-sized noble metal particles. *J Phys Chem B* 102(36):6958–6967
- Huang SM, Hong MH, Luk'yanchuk BS, Chong TC (2003) Direct and subdiffraction-limit laser nanofabrication in silicon. *Appl Phys Lett* 82:4809–4811
- Jain PK, Huang X, El-Sayed I, El-Sayed M (2008) Noble metals on the nanoscale: optical and photothermal properties and some applications in imaging, sensing, biology and medicine. *Acc Chem Res* 41:1578–1586
- Jerisch J, Dickmann K (1996) Nanostructure fabrication using laser field enhancement in the near field of a scanning tunneling microscope tip. *Appl Phys Lett* 68:868–870
- Johnson PB, Christy RW (1972) Optical constants of the noble metals. *Phys Rev B* 6:4370–4379
- Kelly K, Coronado E, Zhao L, Schatz G (2003) The optical properties of metal nanoparticles: the influence of size, shape, and dielectric environment. *J Phys Chem B* 107: 668–677
- Kerker M (1969) The scattering of light and other electromagnetic radiation. Academic Press, New York
- Khlebtsov B, Zharov VI, Melnikov A, Tuchin V, Khlebtsov N (2006) Optical amplification of photothermal therapy with gold nanoparticles and nanoclusters. *Nanotechnology* 17:5167–5179
- Kik PG, Martin AL, Maier SA, Atwater HA (2002) Metal nanoparticle arrays for near-field optical lithography. *Proc SPIE* 4810:7–14
- Kreibig U, Vollmer M (1995) Optical properties of metal clusters. Springer, Berlin
- Lal S, Clare SE, Halas NJ (2008) Nanoshell-enabled photothermal cancer therapy: impending clinical impact. *Acc Chem Res* 41:1842–1851

- Leiderer P, Bartels C, König-Birk J, Mosbacher M, Boneberg J (2004) Imaging optical near-fields of nanostructures. *Appl Phys Lett* 85:5370–5372
- Link S, El-Sayed MA (1999) Spectral properties and relaxation dynamics of surface plasmon electronic oscillations in gold and silver nanodots and nanorods. *J Phys Chem B* 103:8410–8426
- Liu H, Chen D, Tang F, Du G, Li L, Meng X, Liang W, Zhang Y, Teng Xu, Li Y (2008) Photothermal therapy of Lewis lung carcinoma in mice using gold nanoshells on carboxylated polystyrene spheres. *Nanotechnology* 19:455101
- Loo Ch, Hirsch L, Lee M, Chang E, West J, Halas N, Drezek R (2005) Gold nanoshell bioconjugates for molecular imaging in living cells. *Opt Lett* 30:1012–1014
- Matsui I (2005) Nanoparticles for electronic device applications: a brief review. *J Chem Eng Jpn* 38:535–546
- Messenger BJ, Ulrich von Raben K, Chang RK (1981) Local fields at the surface of noble-metal microspheres. *Phys Rev B* 24:649–657
- Mie G (1908) Beiträge zur Optik trüber Medien, speziell kolloidaler Metallösungen. *Ann Phys (Leipzig)* 25:376–445 (in German)
- Miyaniishi T, Sakai T, Nedyalkov NN, Obara M (2009) Femtosecond-laser nanofabrication onto silicon surface with near-field localization generated by plasmon polaritons in gold nanoparticles with oblique irradiation. *Appl Phys A* 96:843–850
- Nedyalkov N, Sakai T, Miyaniishi T, Obara M (2006a) Near field properties in the vicinity of gold nanoparticles placed on various substrates for precise nanostructuring. *J Phys D* 39:5037–5042
- Nedyalkov N, Takada H, Obara M (2006b) Nanostructuring of silicon surface by femtosecond laser pulse mediated with enhanced near-field of gold nanoparticles. *Appl Phys A* 85:163–168
- Nedyalkov NN, Atanasov PA, Obara M (2007a) Near-field properties of a gold nanoparticle array on different substrates excited by a femtosecond laser. *Nanotechnology* 18:305703
- Nedyalkov N, Miyaniishi T, Obara M (2007b) Enhanced near field mediated nanohole fabrication on silicon substrate by femtosecond laser pulse. *Appl Surf Sci* 253:6558–6562
- Palik ED (1998) Handbook of optical constants of solids. Academic Press, San Diego
- Papavassiliou GC (1979) Optical properties of small inorganic and organic metal particles. *Prog Solid State Chem* 12:185–271
- Park JB, Jaeckel B, Parkinson BA (2006) Fabrication and investigation of nanostructures on transition metal dichalcogenide surfaces using a scanning tunneling microscope. *Langmuir* 22:5334–5340
- Plech A, Leiderer P, Boneberg J (2008) Femtosecond laser near field ablation. *Laser Photon Rev* 2:1–17
- Prodan E, Nordlander P, Halas NJ (2003) Electronic structure and optical properties of gold nanoshells. *Nano Lett* 3:1411–1415
- Pustovalov VK (2005) Theoretical study of heating of spherical nanoparticle in media by short laser pulses. *Chem Phys* 308:103–108
- Pustovalov VK, Babenko VA (2005) Computer modeling of optical properties of gold ellipsoidal nanoparticles at laser radiation wavelengths. *Laser Phys Lett* 2:84–88
- Quinten M (1995) Local fields and Poynting vectors in the vicinity of the surface of small spherical particles. *Z Phys D* 35:217–224
- Schleunitz A, Steffes H, Chabicovsky R, Obermeier E (2007) Optical gas sensitivity of a metaloxide multilayer system with gold-nano-clusters. *Sens Actuators B* 127:210–216
- Shirma P, Brown S, Walter G, Santra S, Moudgil B (2006) Nanoparticles for bioimaging. *Adv Colloid Interf Sci* 123:471–485
- Taflove A, Hagness SC (2000) Computational electrodynamics: the finite-difference time-domain method. Artech House, Boston
- Vial A, Grimault AS, Macias D, Barchiesi D, Chappelle MI (2005) Improved analytical fit of gold dispersion: application to the modeling of extinction spectra with a finite-difference time-domain method. *Phys Rev B* 71:085416
- Vo-Dinh T (2003) Biomedical photonics handbook. CRC Press, New York
- Vogel A, Noack J, Hüttmann G, Paltauf G (2007) Mechanisms of femtosecond laser nanoprocesing of biological cells and tissues. *J Phys Conf Ser* 59:249–254
- Volkov AN, Sevilla C, Zhigilei LV (2007) Numerical modeling of short pulse laser interaction with Au nanoparticle surrounded by water. *Appl Surf Sci* 253:6394–6399
- von Allmen M (1987) Laser-beam interactions with materials. Physical principles and applications. Springer, Berlin
- Wang ZB, Luk'yanchuk BS, Hong MH, Lin Y, Chong TC (2004) Energy flow around a small particle investigated by classical Mie theory. *Phys Rev B* 70:035418
- Wellershoff S, Hohlfeld J, Güdde J, Matthias E (1999) The role of electron–phonon coupling in femtosecond laser damage of metals. *Appl Phys A* 69:S99–S107
- Zharov VP, Kim J, Curiel DT, Everts M (2005a) Self-assembling nanoclusters in living systems: application for integrated photothermal nanodiagnostics and nanotherapy. *Nanomedicine* 1:326–345
- Zharov VP, Letfullin RR, Galitovskaya EN (2005b) Micro-bubbles-overlapping mode for laser killing of cancer cells with absorbing nanoparticle clusters. *J Phys D* 38:2571–2581
- Zheng X, Xu W, Corredor Ch, Sh Xu, An J, Zhao B, Lombardi JR (2007) Laser-induced growth of monodisperse silver nanoparticles with tunable surface plasmon resonance properties and a wavelength self-limiting effect. *J Phys Chem C* 111(41):14962–14967